THE STRUCTURE OF FLUID AND GLASSY SYSTEMS AT SHORT TIME AND LENGTH SCALES

by

ANDREW P. HAMMOND

A DISSERTATION

Presented to the Department of Physics
and the Graduate School of the University of Oregon
in partial fulfillment of the requirements
for the degree of
Doctor of Philosophy

December 2019

DISSERTATION APPROVAL PAGE

Student: Andrew P. Hammond

Title: The Structure of Fluid and Glassy Systems at Short Time and Length Scales

This dissertation has been accepted and approved in partial fulfillment of the requirements for the Doctor of Philosophy degree in the Department of Physics by:

Raghuveer Parthasarathy	Chair
Eric Corwin	Advisor
Ben McMorran	Core Member
Marina Guenza	Institutional Representative

and

Kate Mondloch	Interim Vice Provost and Dean of the Graduate School

Original approval signatures are on file with the University of Oregon Graduate School.

Degree awarded December 2019

DISSERTATION ABSTRACT

Andrew P. Hammond

Doctor of Philosophy

Department of Physics

December 2019

Title: The Structure of Fluid and Glassy Systems at Short Time and Length Scales

All constituent particles of material at non-zero temperature undergo ballistic motion at a short enough timescale. At longer times the particles begin to interact with the other constituent particles forcing them to transition out of the ballistic regime. The manner in which a particle transitions out of ballistic motion is a useful probe of the micro-scale material structure. Here, I develop an experimental setup that allows me to track a particle with sufficient spatial and temporal resolution to distinguish the ballistic motion and the subsequent transition to the long time structural behavior. I verify this technique by analyzing the motion of a freely floating colloid in water and comparing it's ballistic diffusive transition to the accepted behavior for a Newtonian liquid. I extend this treatment to a colloid suspended in a Maxwell fluid. I prove that the liquid's micro-scale behavior is qualitatively the expected behavior for a Maxwell liquid while deviating significantly from the quantitative picture. Next, I examine the motion of a colloid within a dense colloidal glass. I demonstrate that there are three different structural behaviors present in the system depending on the packing density. Further, these different phases precisely align with those predicted by the replica

theory of glasses for a dense liquid, a stable glass, and a marginal glass. This constitute the first experimental proof of the existence of a marginal glass and an important confirmation of the replica theory of glasses. This work also begins to experimentally map the colloidal glass phase diagram revealing a reentrant stable glass phase space.

This dissertation includes previously published and unpublished co-authored material.

CURRICULUM VITAE

NAME OF AUTHOR: Andrew P. Hammond

GRADUATE AND UNDERGRADUATE SCHOOLS ATTENDED:
University of Oregon, Eugene, OR
Reed College, Portland, OR

DEGREES AWARDED:
Doctor of Philosophy, Physics, 2019, University of Oregon
Bachelor of Arts, Physics, 2010, Reed College

AREAS OF SPECIAL INTEREST:
Soft Condensed Matter, Granular Materials, Active Matter, Biophysics

PROFESSIONAL EXPERIENCE:

Research Assistant, Physics, University of Oregon, 2016-2019

Teaching Assistant, Physics, University of Oregon, 2013-2016

Accelerator Systems Operator, SLAC National Accelerator Laboratory, 2010 - 2013

Teaching Assistant, Reed College, 2008 - 2010

GRANTS, AWARDS AND HONORS:

APS Soft Matter Travel Award, American Physical Society, 2017

First-Year Fellowship Award, University of Oregon, 2013

PUBLICATIONS:

A. P. Hammond & E. I. Corwin, "Direct measurement of ballistic to diffusive crossover in colloidal particles in simple and complex fluids" *Physical Review E*, **96**, 042606 (2017).

A. P. Hammond & E. I. Corwin, "Seeing through a glass clearly: Experimentally observing the marginal glass phase" Submitted *PNAS*, (2019).

ACKNOWLEDGEMENTS

I'd like to first thank my parents and brother and sister for their support. I would like to thank my advisor Eric Corwin for his guidance, advice, and friendship. I would also like to thank Raghu Parthasarathy for his many helpful discussions, his willingness to let me use his microscopes, and the proofreading he performed on my papers. The UO machine shop staff, in particular John Boosinger were also extremely helpful for this work. Finally, I would like to thank my lab mates, in particular Peter Morse, Kyle Welch, Yasin Karim, Alex Trevelyan, Cameron Dennis, James Sartor, Francesco Arceri, and Varda Faghir Hagh for their many useful comments. This work was supported by National Science Foundation (NSF) Career Award DMR-1255370, and the Simons Foundation No. 454939.

TABLE OF CONTENTS

Chapter Page

LIST OF FIGURES

Figure Page

CHAPTER I

INTRODUCTION

When you throw a rock into a pond you generally get a nice splash as the rock causes the water to deform around it. This is because a rock is a solid and water is a liquid. Indeed the physical distinction between a liquid and a solid is that when subjected to a shear stress, liquids deform continuously and solids don't. However, it is also possible to skip a rock over the surface of a pond, almost like water was behaving like a solid. This example demonstrates that the rigid distinction between liquids and solids is far more fluid than commonly thought.

Over the course of my studies I have found a number of different materials that fill in the spectrum between liquids and solids. These range from material like pitch, which appear solid-like at short time scales but are actually liquids as demonstrated in the hundred year pitch drop experiments [1], or more complex materials like toothpaste and mayonnaise which have a definite shape but can flow as well. There are also solids like sand which can exhibit properties typically associated with liquids. If you pick up a handful of sand it feels solid, but when you relax your hand it flows like water. These materials that stand between liquid and solid fascinate me. They are all made up of atoms but because of the different structures of those materials they have a variety of different macro-scale behaviors.

When probing these materials, I started with the thing that unites them: they are all made up of discrete units, whether the particles are atoms, molecules, grains of sand, or even colliding pool balls. Also, all of these materials motion and by extension structure is best understood by examining their thermodynamics; in short they are thermal materials. Thermal materials have the property that each

constituent particle is, at the shortest length scale, moving with a constant velocity in a constant direction. This is exactly the motion of a pool ball between collisions. However, eventually, each of these particles experience a collision causing them to begin to interact with their environments and to begin to develop a structural identity. It is this period which I decided to focus on, the transition from ballistic to the material's first structural behavior.

These considerations motivated me to design and build an experimental apparatus to observe a particle, in my case a tracer colloid, transition out of ballistic motion. While starting at the first structural time scale is an obvious place to start, it is not an easily accessible experimental time scale. In addition, the length scale is quite small requiring nano-scale precision. Indeed, for my system in water the time scale is 0.36ms and the length scale is 4nm. The problem of both small length and short time scales as well as the numerous sources of noise that inevitably creep into an experiment combined to halt previous attempts to make this measurement. Only recently were any experiments performed which tracked an individual particle's ballistic motion [2, 3, 4, 5]. These experiments used a laser trap to hold a tracer particle in a small area to accurately measure the ballistic motion with a high-speed camera, however the use of a laser trap greatly diminishes their ability to measure longer range motion. Therefore, I had to modify there setup. I used a high-speed camera combined with high intensity illumination in a bright field microscope. I also opted for colloids with a diameter of around 50 μm because this is big enough to track at the required precision while clearly experiencing thermal ballistic motion. The colloids were individually tracked using a tracking algorithm [6] which I modified slightly to focus on the larger colloids. Using these techniques and equipment, I was able to observe the ballistic transition,

the first time this has been achieved for an unconfined colloid. Appendix 1 gives a more in depth examination of the experimental setup with a particular emphasis on trouble shooting various problems that might crop up.

Once I created an experimental apparatus, I examined the transition between ballistic and diffusive motion in water [7, 8, 9, 10, 11, 12]. I successfully tracked a series of colloids as they experienced both ballistic and diffusive motion. Using the colloids trajectories, I calculated a mean squared displacement (MSD) to better analyze the properties of the colloids transition from ballistic to diffusive motion. With the MSD, I was able to fit my experimental data with the Clercx-Schram equation [12] the MSD derived from theoretical models and verified using computer simulations. The data fit the Clercx-Schram equation with a high degree of accuracy verifying the experimental techniques I employed. From here, I expanded on this demonstrated success to examine the structure of a Maxwell fluid, a non-Newtonian fluid that behaves like a solid at intermediate time scales. This experiment is detailed in Chapter 2 and was published in *Physical Review E* [13].

After examining the ballistic and diffusive transition in several liquids, I decided to expand this technique to look at glasses. This constitutes a fairly large shift. Whereas in the previous work I was using a colloid to examine the structure of the suspending liquid, here I created a colloidal glass [14, 15, 16, 17] by taking a large number of colloids with a few tracer colloids mixed in and then add an interstitial liquid. The interstitial liquid, which was designed to have the same density and refractive index as the colloids, serves to both increase the transition time scale and to reveal the tracer colloids deep within the other colloids. Therefore, the colloids are not just probes, but form an integral part of

the system's structure. This is useful not only as a relevant system all on its own to talk about glasses, but also is a useful model for molecular glasses. Using this system I found that the tracer colloid behaved in three different ways depending on the density of the colloidal packing: 1) the MSD transitioned from ballistic to sub-diffusive motion, 2) the MSD moved from ballistic to a flat plateau , and 3) the MSD started ballistically and then grew logarithmically at long times. I interpreted these changes using the replica theory of glasses [18, 19, 20, 21, 22, 23, 24, 25] as corresponding to three different phases: glassy liquid, stable glass, and marginal glass. My results constitute the first thermal experimental evidence for the existence of the marginal glass phase. Chapter 3, which has been submitted to *PNAS*, expands on these points providing a full discussion of the experiment.

CHAPTER II

DIRECT MEASUREMENT OF THE BALLISTIC MOTION OF A FREELY FLOATING COLLOID IN NEWTONIAN AND VISCOELASTIC FLUIDS

2.1. Abstract

A thermal colloid suspended in a liquid will transition from a short time ballistic motion to a long time diffusive motion. However, the transition between ballistic and diffusive motion is highly dependent on the properties and structure of the particular liquid. We directly observe a free floating tracer particle's ballistic motion and its transition to the long time regime in both a Newtonian fluid and a viscoelastic Maxwell fluid. We examine the motion of the free particle in a Newtonian fluid and demonstrate a high degree of agreement with the accepted Clercx-Schram model for motion in a dense fluid. Measurements of the functional form of the ballistic-to-diffusive transition provide direct measurements of the temperature, viscosity, and tracer radius. We likewise measure the motion in a viscoelastic Maxwell fluid and find a significant disagreement between the theoretical asymptotic behavior and our measured values of the microscopic properties of the fluid. We observe a greatly increased effective mass for a freely moving particle and a decreased plateau modulus.

This work was originally published in *Physical Review E* [13]. The writing and analysis were performed by me as primary author. Eric Corwin is listed as a coauthor as he advised this work.

2.2. Introduction

At very short time and length scales the diffusive motion of a Brownian particle breaks down into a series of individual ballistic flights. The functional form of this transition is controlled by the microscopic structure and behavior of the fluid. The microscopic time and length scales for the ballistic motion are so small that direct measurements have only recently become possible [2, 4, 5, 26]. These experiments have used optical traps to confine a test particle within a harmonic well, allowing a high precision measurement of the short time motion but at the cost of a loss of information about the crossover to longer time behavior that is indicative of the microscopic structure of the fluid. Furthermore, laser traps by their nature create a harmonic potential energy well for the motion of the particle and thus function similarly to an elastic term in a viscoelastic fluid. As such, it can be difficult to deconvolve the effect of the trap from the effects of the elastic component of the fluid. Indeed, all studies of viscoelastic fluids known to the authors don't address the ballistic regime. Here we avoid the limitations and contaminations caused by the use of a laser trap and present direct measurements of the full transition away from ballistic motion for a freely moving colloid suspended in simple Newtonian and viscoelastic Maxwell fluids. These measurements are achieved in an interaction free manner using a high speed camera, intense illumination, and an accurate tracking algorithm [6]. These measurements allows us to unambiguously distinguish between microscopic models for dense fluid thermal motion [7, 8, 9, 10, 11, 12, 27, 28, 29, 30] and provide a hithertofore impossible glimpse into the fundamental behavior of thermal fluids. In a simple Newtonian fluid, our measurement is in close correspondence with analytic predictions. By fitting our data we can directly measure the constants

of motion as well as a first principles measurement of the temperature of the fluid. Having proven the validity of this method, we experimentally examine the motion of a single particle in a Maxwell fluid as it transitions from ballistic to elastically trapped to diffusive motion, the first observation of this kind. We compare these results to existing microscopic models for Maxwell fluids [27, 30, 31, 32], and find significant discrepancies between the model predictions and the observed behavior.

An early effort to model the ballistic diffusive transition was performed with the ideal gas approximation [7, 8] given by:

$$\left\langle x^2 \right\rangle = 2k_B T \frac{m}{\gamma^2}\left(\frac{t\gamma}{m} - 1 + e^{-t\gamma/m}\right), \tag{2.1}$$

Here γ is the Stokes value ($6\pi r\eta$), k_B the Boltzman constant, T the temperature, η the viscosity, r the tracer radius and m is the mass of the colloid. A more accurate model for dense fluids, motivated by early computer simulations [33, 34], was achieved by adding an effective mass term and a memory term to the ideal gas model [9, 11]. The effective mass term models the frictionally bound fluid that is attached to the particle and the memory term models the inertial interaction of the particle with nearby moving fluid [35]. At sufficiently short timescales and close to the speed of sound in the fluid this model breaks down and is replaced with the simple ideal gas model. The memory term in the dense fluid model, comes from the entrained fluid in a dense sytem which slows the change of direction.

These modifications to the Langevin equation were analytically solved [12] under the assumptions that the fluid is viscous and incompressible, the Reynolds number is low, and the test particle is a hard sphere [10, 36]. The predicted MSD is

given by:

$$\left\langle x^2 \right\rangle = \frac{2k_BT}{\gamma}\left(t - \frac{2z}{\gamma\sqrt{\pi}}\sqrt{t} + \frac{z^2-\gamma M}{\gamma^2} + \frac{\gamma}{M\left(b-a\right)}\times \right.$$
$$\left.\left(\exp\left(b^2t\right)\operatorname{erfc}\left(b\sqrt{t}\right)b^{-3} - \exp\left(a^2t\right)\operatorname{erfc}\left(a\sqrt{t}\right)a^{-3}\right)\right) \tag{2.2}$$

For simplicity's sake we define constants z, a, and b as

$$z = 6\pi r^2\sqrt{\rho\eta} \tag{2.3a}$$
$$a = \left(z + \sqrt{z^2 - 4\gamma M}\right)/2M \tag{2.3b}$$
$$b = \left(z - \sqrt{z^2 - 4\gamma M}\right)/2M \tag{2.3c}$$

where M is the effective mass which is $m + \frac{1}{2}m_f$, where $m_f = \frac{4}{3}\pi r^3\rho$ is the the mass of the fluid displaced by the colloid, and ρ is the density of the fluid. A sample MSD is plotted in figure 2.2. The dense fluid model and the ideal gas model both share similar asymptotic forms. At short times, known as the ballistic regime, the MSD asymptotes to $(2k_BT/M)t^2$. At long times, the diffusive regime, the MSD scales as $(4k_BT/\gamma)t$. The dense fluid MSD differs from the ideal gas MSD in two salient ways: 1) It gives rise to a slower ballistic velocity, caused by the increased effective mass of the particle. 2) It has a much gentler crossover between ballistic and diffusive motion, caused by the inertial memory of the liquid.

Non-Newtonian fluids, however, have much more complicated Langevin equations [27, 30] which have not been explored as intensely due to the lack of experimental data at the shortest length and time scales. One of the simplest non-Newtonian fluids is a Maxwell fluid, characterized by a single terminal relaxation time between spring like and viscous like behavior. This requires the addition of

a decaying spring term to the Langevin equation. This additional term results in an intermediate plateau regime in the MSD corresponding to the behavior of a thermal spring. While analytical solutions for the Maxwell fluid are lacking, predictions have been made about the asymptotic behavior in the three regimes: ballistic motion, elastically trapped motion, and finally diffusive motion. The short-time ballistic behavior is predicted to asymptote to $(2k_BT/m)t^2$, the elastic trap should have a constant MSD of $2k_BT/\pi rG_0$, and the long-time diffusive motion is predicted to have an asymptote of $(4k_BT/\gamma)t$ [27]. Here G_0 is the plateau modulus, a commonly measured rheological value which measures the amplitude of the storage and loss moduli [37]. We use our technique to test the rheological predictions when applied to a single unconstrained particle in such a fluid moving between ballistic and diffusive regimes.

2.3. Methods

In this experiment, we used polystyrene hard spheres with a radius of 21.8 μm as our tracer particle. Polystyrene was chosen because it is easily density matched to water using NaCl with only minimal, and known, changes to the viscosity. The size of the particle, larger than those in optical trap experiments, was chosen because the tracking precision as well as the ideal gas transition time and length increase with increasing radius. We chose to use water as our experimental liquid because of its ubiquity in experiments and its relatively low viscosity. For our setup, the Reynolds number is 2.4×10^{-9}. This system fulfills all of the underlying assumptions required by the dense fluid equation. When selecting a Maxwell fluid we chose to use a solution of Cetyltrimethylammonium chloride (CTAC) mixed with water. This mixture has been found to exhibit a Maxwell fluid behavior

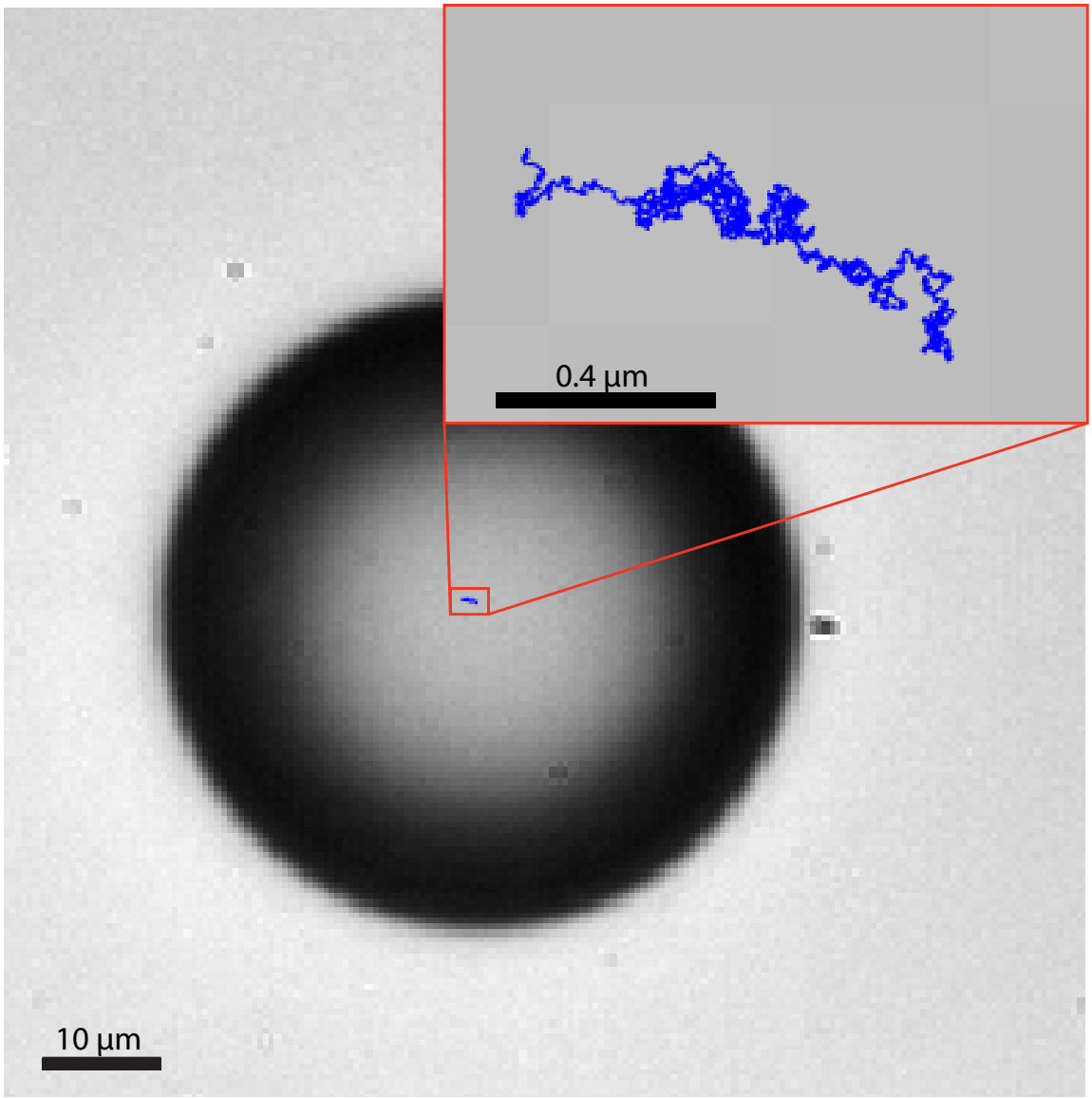

FIGURE 2.1. Suspended colloid and path
A single colloid suspended in water viewed through the microscope. The path the particle travels for the next 2 seconds is shown in blue.

caused by worm-like micelles [28, 38] and is a commonly studied Maxwell fluid. The micelles formed produce a network within the fluid. This network, acting together, changes the properties of the supporting fluid. Because the test particle we use is larger than the micelles it will probe the properties of the complex fluid rather than solely those of the intervening fluid.

Test particles were placed into a deionized water mixture at 5×10^{-3} % w/v of colloid. The colloids are slightly denser than water, so NaCl was added to density match the system at a measured value of 1.06×10^3 kg/m^3. After sonicating and degassing the colloid-water solution, it was placed in a Fastwell silicon spacer cavity between a slide and a cover slip. The chamber was sealed with vacuum grease to ensure that air bubbles did not form. The silicon spacer had a width of 2.4 mm and circular void with a radius of 5 mm allowing the colloids to be imaged far from wall effects. The slides were cleaned with piranha solution and dried with nitrogen gas, which removed any coatings on the slides.

We created a Maxwell fluid using a solution of CTAC at 1% by weight with water with the addition of 0.12 M of NaSal to facilitate the formation of micelles. We directly measured the plateau modulus of this solution to be 5.72 Pa using an angular frequency sweep from 62 - 0.062 rad/s at a constant displacement of 0.18 mrad (TA Instruments AR-2000ex rheometer, with a 60mm 1.025° cone plate). Our fluid had a density of 1.055×10^3 kg/m^3, slightly lower than the average density of the beads. However, the density is close enough that beads did not fall out of suspension until well after all the measurements were complete. The same test particles were added at a concentration of 2.5×10^{-3} % w/v. When preparing samples, we used a process almost identical to the one for water. The major difference was that the sample was not sonicated ahead of being added to

the Fastwell because the fluid solidified when exposed to high frequency agitation. Instead, the sample was slowly mixed using a low frequency mixer.

All data was collected on a Nikon TE2000s microscope on a floating stage optical table in a climate controlled room. Illumination was provided by a 500mW red LED (Thorlabs LED635L) shining through the microscope condenser. In between the LED and sample a neutral density filter on a swivel mount was added to allow initial setup to be done without excessive local heating of the sample. The sample was encased in a small cardboard box for isolation from acoustic vibrations. Images were gathered through a 50x lens (Nikon LU plan ELWD 50x/0.55 B inf/0 WD 10.1) using a Phantom M310 high speed camera. Videos were taken at 40,000 fps (T = 25 μs) with an image size of 192x192 pixels and a magnification of 0.4μm/pix. When filming a particle all motorized elements on the microscope and camera were turned off to eliminate small vibrations. Once a particle was found, filming lasted 2.84 s (113,600 frames) after which the LED was immediately shut off and the ND filter replaced.

We used a radial center tracking algorithm[6] to find the center of the colloids in progressive frames of the video. Using a combination of simulations and tracking test particles which were stuck to the slide, we found that the algorithm did not exhibit a preferred direction. We found that the mean position error was about 1.5 nm in each frame. A representative trace with the first video frame is shown in figure 2.1.

Because of the very large number of frames, the precision of the individual measurement is only a significant source of error for small measurements. In addition to the measurement error, the finite nature of our sample size introduces additional errors for long times. The total error is at each lag-time τ is calculated

as:

$$\sigma_V(\tau) = \sqrt{\frac{8\sigma_p^2 \mathrm{Var}(\tau)}{N(\tau)} + \frac{16\sigma_p^4}{N(\tau)} + \frac{\mathrm{Var}(\tau)^2}{N_{ind}(\tau)}}, \tag{2.4}$$

where σ_V is the standard deviation (STD) of the variance, σ_p the STD of the position, N the total number displacements measured given by $(\Gamma - \tau) \times f$ with Γ the total time and f the frequency, and N_{ind} the number of independent steps $(\Gamma - \tau)/\tau$.

2.4. Results

We calculate the mean squared displacement (MSD) from our measured data as $\mathrm{MSD}(\tau) = \langle \|\vec{x}(t+\tau) - \vec{x}(t)\|^2 \rangle$ where $\vec{x}(t)$ is the measured position of the particle at time t, τ is the lag-time between position measurements, and angle brackets denote a time average. The MSD for a representative particle is plotted as green squares in figure 2.2. This MSD exhibits a small drift at long times, past about 0.1 s, and a noise floor at very short times. The drift is likely the result of convective flows within our sample chamber, driven, perhaps, by local heating of the sample. However, this drift can be easily removed by calculating the variance of particle position as a function of lag time as $\mathrm{Var}(\tau) = \mathrm{MSD}(\tau) - \|\langle \vec{x}(t+\tau) - \vec{x}(t) \rangle^2\|$. The noise floor is caused by photon shot noise in our camera contributing to uncertainty in the localization of a particle. We can directly measure this noise by tracking a particle fixed to a slide and find it to be independent and identically distributed Gaussian noise with a variance of approximately 2×10^{-18} m^2 (inset to figure 2.2). The precise value of this noise variance changes from run to run due to variations in particle size and particle focus (due to changes in z-position). Because this noise is independent and identically distributed for a given measurement we can simply

subtract the noise floor from our measurement to find the true variance of our particle, plotted as black circles in figure 2.2.

The plotted variance clearly shows a ballistic regime below about 10^{-3} to 10^{-4} s, a crossover regime up till about 10^{-2} s, and a diffusive regime for longer times. The measured variance fits the dense fluid model exceedingly well over the entire range of measured lag-times as shown in figure 2.2. The model depends on four physical parameters: 1) temperature, 2) particle radius, 3) fluid density, and 4) fluid viscosity. Of these, we independently measure the fluid density prior to observation. The fluid viscosity of salt water is a known function of density and the temperature [39]. Therefore, we have only two independent fitting parameters: temperature and particle radius. To this, we add a third fitting parameter to describe the magnitude of the noise floor.

We independently fit 18 measurements using 18 different particles, shown in figure 2.3. On average, the particle radius was found to be 20.5 $\pm$ 0.8 μm, within tolerance of the manufacturer's quoted radius. The average temperature measured by our fitting was found to be slightly higher (297 $\pm$ 4.5 K) than the measured room temperature (293 $\pm$ 2 K), likely the result of local heating from the intense illumination. The noise floors for the measurement were found to range from 1.2×10^{-18} m^2 to 2.4×10^{-18} m^2. Thus fit, the dense fluid functional form is indistinguishable from the data over much of our measured range. To characterize the agreement, we plot the residual percentages, and find them to be unbiased and with error less than 5% over at least two decades of lag time, as shown in figure 2.3. At longer times, where drift and sampling errors increase, the percent error increases as well.

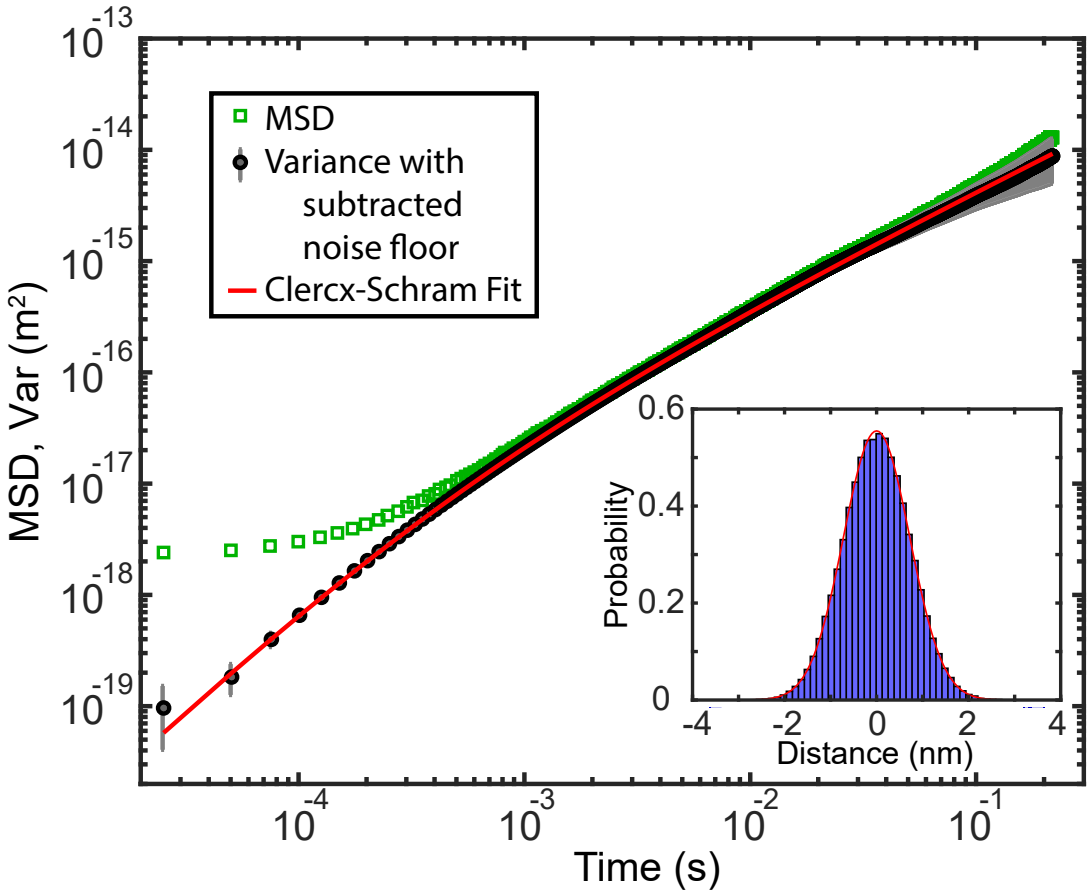

FIGURE 2.2. Experimental variance and fit in water
The variance of the colloid's trace, shown in figure 2.1. The green squares show the mean squared displacement. The black dots with the error bars show the variance with the noise floor subtracted, in this case 2.34×10^{-18} m^2. In red is the fitted Clercx-Schram theoretical prediction for the MSD. The best fit value for Temperature is 302 K, and for radius 21 μm. We propagate the localization error of the position measurement as well as sampling error through our calculation to obtain error bars for the plot as described in the supplementary material. Inset: A histogram of measured positions for a stranded particle.

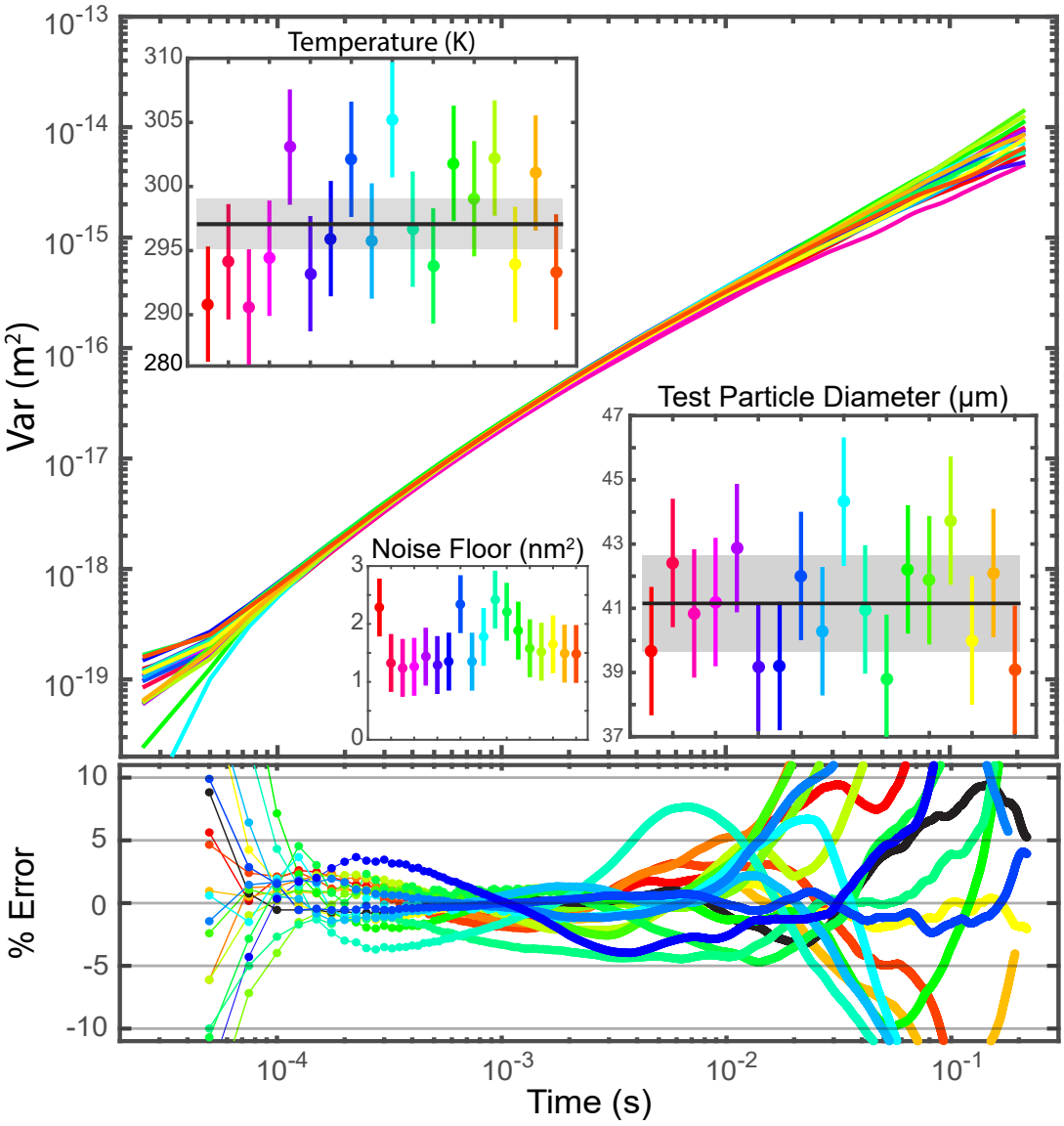

FIGURE 2.3. Fitted temperature and diameter with Residual Percentages Top: The noise floor adjusted variance for 18 different videos. Inset: The fitted temperature, test particle radius, and noise floor for the different trials. The black line shows the mean values with a gray standard deviation. Bottom: Residual percentages showing by what percent the measurement deviates from the individual fits for each of the corresponding variance's shown above.

We perform similar experiments in a Maxwell fluid created with a solution of CTAC and water as described above. As in the case with water, we see a minimum noise floor at short times and a long time drift in the MSD. The drift in the measurement is removed by using the variance as described above and the noise floor is estimated and subtracted as shown in Figure 2.4 for a representative trial. In total 30 independent measurements were made with this Maxwell fluid.

The plotted variance for a Maxwell fluid has two notable features. 1) At short times the motion is clearly ballistic. The best fit prefactor for the asymptote is however considerably lower than the one predicted by either the ideal gas or dense fluid models, corresponding to an effective mass six times larger than the particles mass or an entrained region with a radius $39.6\mu m$, compared to the reported radius of $21.8\mu m$. This increased effective size of the particle can perhaps be understood as a result of the fact that the surrounding fluid contains a network of worm-like micelles. The test particle impinges upon the network of intertwined micelles and pulls some of them along thus increasing the particle's effective mass. Alternatively, the surface of the particle may actually attract the micelles which would increase the effective mass as well. However, due to the presence of salt in this solution any interaction between the particle and the micelles must necessarily be small. 2) The variance shows a clear secondary plateau which is independent of the noise floor. This plateau is characteristic of thermally damped motion consistent with a Maxwell fluid's predicted behavior for high frequencies. Examining the best fit asymptotes to the plateau regime, we find an average plateau modulus over all measurements of $16 \pm 2\ Pa$. This is almost a factor of 3 larger than the rheometer measured value of $5.7\ Pa$.

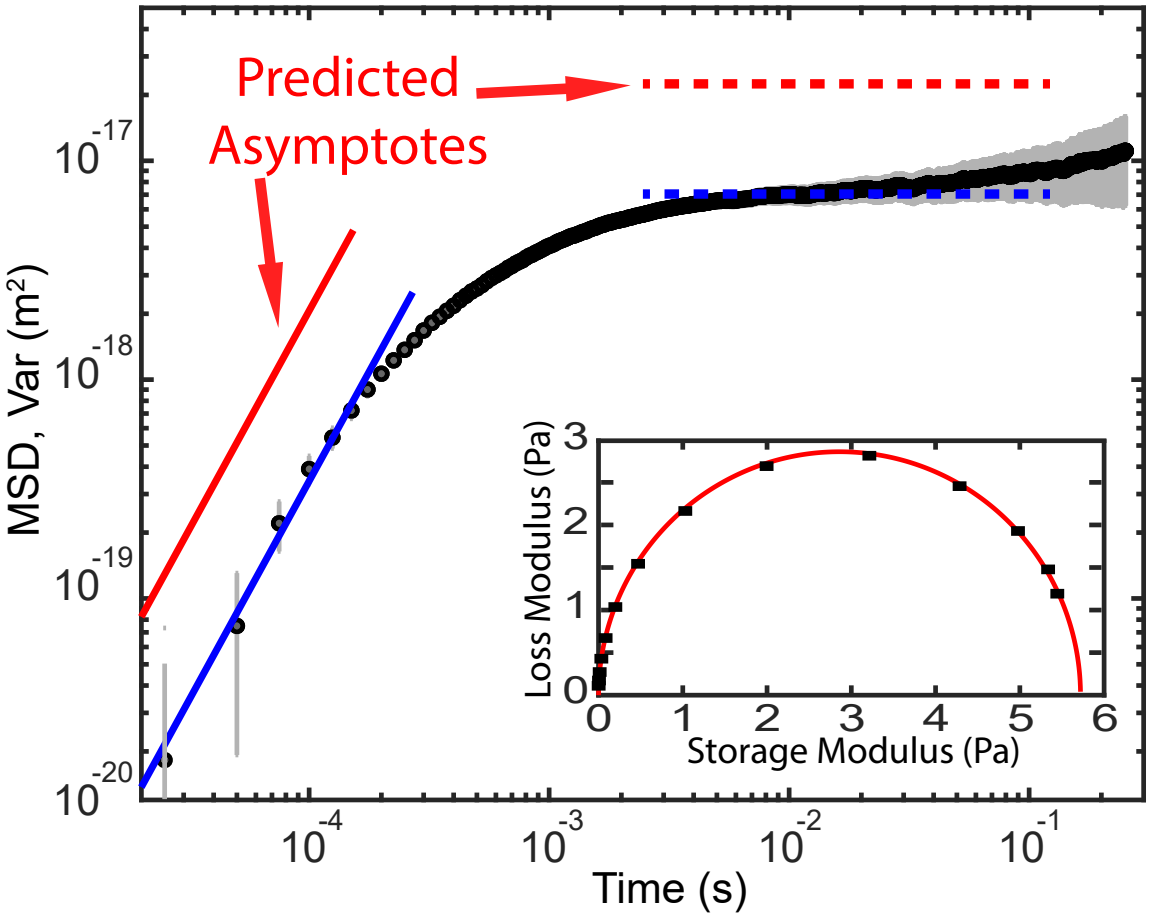

FIGURE 2.4. Experimental variance with asymptotes in Maxwell fluid
The MSD and adjusted variance for a particle moving in a Maxwell fluid. The black dots show the noise floor subtracted variance. In this figure the noise floor used is 2.2883×10^{-18} m^2. The red lines show the predicted theoretical asymptotes [27] for the ballistic (solid) and plateau (dashed) regimes. The blue lines show the observed asymptotes for the ballistic (solid) and plateau (dashed) regimes. Inset: The Cole-Cole plot for CTAC as measured with a conventional rheometer. The red curve is a fit to the Maxwell function demonstrating a measured plateau modulus of 5.72 Pa.

The Cole-Cole plot (inset to Figure 2.4) for this fluid shows it to be a perfect Maxwell fluid when measured on a conventional rheometer, however this deviates from the observed microscopic behavior. These results demonstrate that at the short time and length scales that our technique probes, the physics governing this fluid are in fact significantly more complicated than those of a simple Maxwell fluid model. The displacement scales probed with our technique are just under 4 orders of magnitude smaller than those accessible to a rheometer and the time scales are two orders of magnitude smaller.

2.5. Conclusions

In this experiment, we resolve the functional form of the ballistic crossover, revealing the fundamental length and time scales between individual and collective interactions in both Newtonian and Maxwell fluids. In so doing we have created a micro-scale first-principles thermometer based on the kinetic theory definition of temperature. We have demonstrated the validity of this approach by the extremely precise agreement between our results and theoretical models for motion in dense Newtonian fluids. We have experimentally tested the accuracy of Maxwell fluid Langevin equation solutions and found them to be wanting in accurately describing real materials. Asymptotically, we see a clear need for the addition of an effective mass term. More troublingly, the plateau values as measured with this method are markedly different from those found with a conventional rheometer. This difference may be a sign of a shift in behavior between the microscale addressed by our measurement and the macro-scale measurement performed with a rheometer, suggesting that materials which appear Maxwell at large length scales may be more complicated at small length scales. Alternatively, this result could be indicative

that the assumptions used in deriving the asymptotic behavior of the model need to be further modified. Our technique provides an independent method for testing models for the microscopic structure of fluids and the accompanying macroscopic fluid constants. In the future, this method promises to be useful in measuring multiple transitions between motion regimes in viscoelastic materials, an area where laser traps have difficulty because of the effects of confinement [32]. This method will also enable detailed studies of the influence of long range interactions, such as wall effects, in an interaction free manner [40]. As such, high speed single particle tracking promises to become an important tool in the study of the fundamental behavior of liquids.

CHAPTER III

SEEING THROUGH A GLASS CLEARLY: EXPERIMENTAL OBSERVATION OF THE MARGINAL GLASS PHASE

This work has been submitted to *Nature Physics*. The writing and analysis were performed by me as primary author. Eric Corwin is listed as a coauthor as he advised this work.

3.1. Introduction

Glasses are ubiquitous, yet a first principles theory explaining their properties remains elusive. A snapshot of the configuration of molecules in a glass appears to be the same as that of a dense liquid, yet glasses are solids not liquids. The recently proposed replica theory of glasses has overcome this lack of a structural signature and provides a first principles theory [18, 19, 20, 21, 22, 23, 24, 25]. This theory predicts two distinct glass phases: a stable glass phase, characterized by an energy landscape of multiple disconnected local minima and a marginal glass phase characterized by an energy landscape of fractally dense local minima. The marginal phase has been observed in multiple simulations [41, 42, 43, 44, 45, 46], however, it is not known whether the replica theory is applicable to an experimental glass. Here we show that such a phase does exist in a slowly densifying colloidal glass, providing the first thermal experimental confirmation of the replica theory of glasses. We use the mean squared displacement of individual colloids at extremely short time and length scales as an assay to determine the phase of matter. By observing as a function of density we find evidence for a reentrant marginal phase and can begin to map out the phase diagram for colloidal glasses and compare it

to the mean field result [23, 46]. Our results demonstrate that glasses self organize into a hierarchy of cages characteristic of a marginal phase. The existence of which provides strong evidence for a series of thermodynamic phase transitions underlying the dramatic change in behavior seen between a liquid and a glass. This work provides a blueprint to creating a complete phase diagram for glasses, including behavior deep within the glassy phase. The techniques developed in this work explore a previously underlooked regime for glasses, that of the shortest time and length scales. Measuring behavior in this regime is a potent tool with which to to explore previously inaccessible implications of the mean field theories of glasses and to probe new material properties.

Within the replica theory of glasses, the energy landscape of a stable glass is dominated by distinct local minima contained within smooth basins. A signature for this phase can be found in the mean squared displacement (MSD) of individual particles. As in all thermal systems, at shortest times particles will move ballistically. Because the basin is smooth, particles will rapidly explore their local cage and the MSD will reach a flat plateau characterized by the size of the cage. This signature of the stable glass has been verified both computationally and experimentally [15, 16, 47, 48, 49, 50, 51, 52, 53].

The energy landscape of a marginal glass also known as a gardener phase is superficially similar to that of a stable glass in that it is broken up into multiple basins. However, the energy basin in a marginal glass is itself broken up into a series of fractally dense sub-basins [22, 23, 43, 54, 55]. The system is no longer characterized by perturbations around a particular energy minima, but rather by a constant change of the system's energy minima within a set of sub-basins. Work done on an externally controlled psuedo-thermal two-dimensional disk system

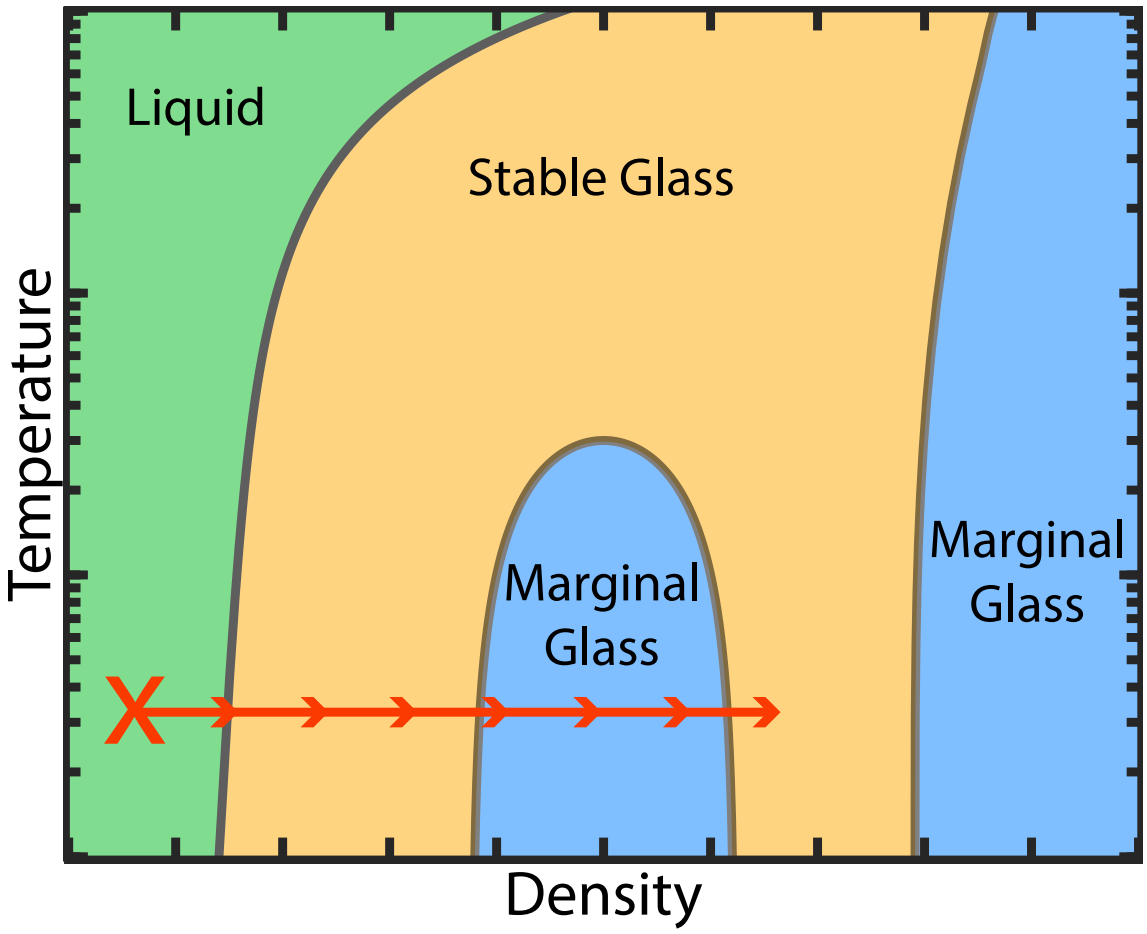

FIGURE 3.1. Glass phase diagram
Sketch of a phase diagram for soft sphere glasses as a function of temperature and density, adapted from [23, 46]. Our experiment starts at the "X" and follows the arrows from the liquid to stable glass to marginal glass and then further into the stable glass phase.

has found evidence of a marginal phase through a direct replica signature similar to that employed in numerical simulations [56]. A study of the Johari-Goldstein Relaxation in sorbitol and xylitol found an extreme broadening of the β relaxation distribution as a structural glass was cooled to very low temperatures, consistent with the fractal roughening of the energy landscape predicted by the marginal phase [57].

A signature for this phase may also be found in the MSD which will be marked by a slow logarithmic growth at longer times as the system is caged within and then successively breaks out of ever larger sub-basins at an ever longer timescale. At shortest times the ballistic motion should be relatively unchanged. Such behavior in the long time limit has been seen in some numerical simulations [23, 42, 43, 45], is absent in others [44, 58], but has never been observed in thermal experiments. Further, due to the high computational cost in numerical simulations, the transition from ballistic to logarithmic behavior in the MSD has never been observed.

In this work we create a colloidal glass and follow it's behavior as it increases in density, characterizing the phase from the MSD signatures. We observe a clear signature of both the stable and marginal phases. We then qualitatively compare these results to the recently proposed re-entrant glassy phase diagram for colloids [23, 46] (Figure 3.1) and find good agreement.

3.2. Methods

Our experimental system consists of nominally 50 μm diameter PMMA colloids (Cospheric PMPMS-1.2 45-53um $>$ 95%) with 95% falling within a range of 45-53 μm, sphericity greater than 99%, and density 1.20 g/cm^3. The degree of

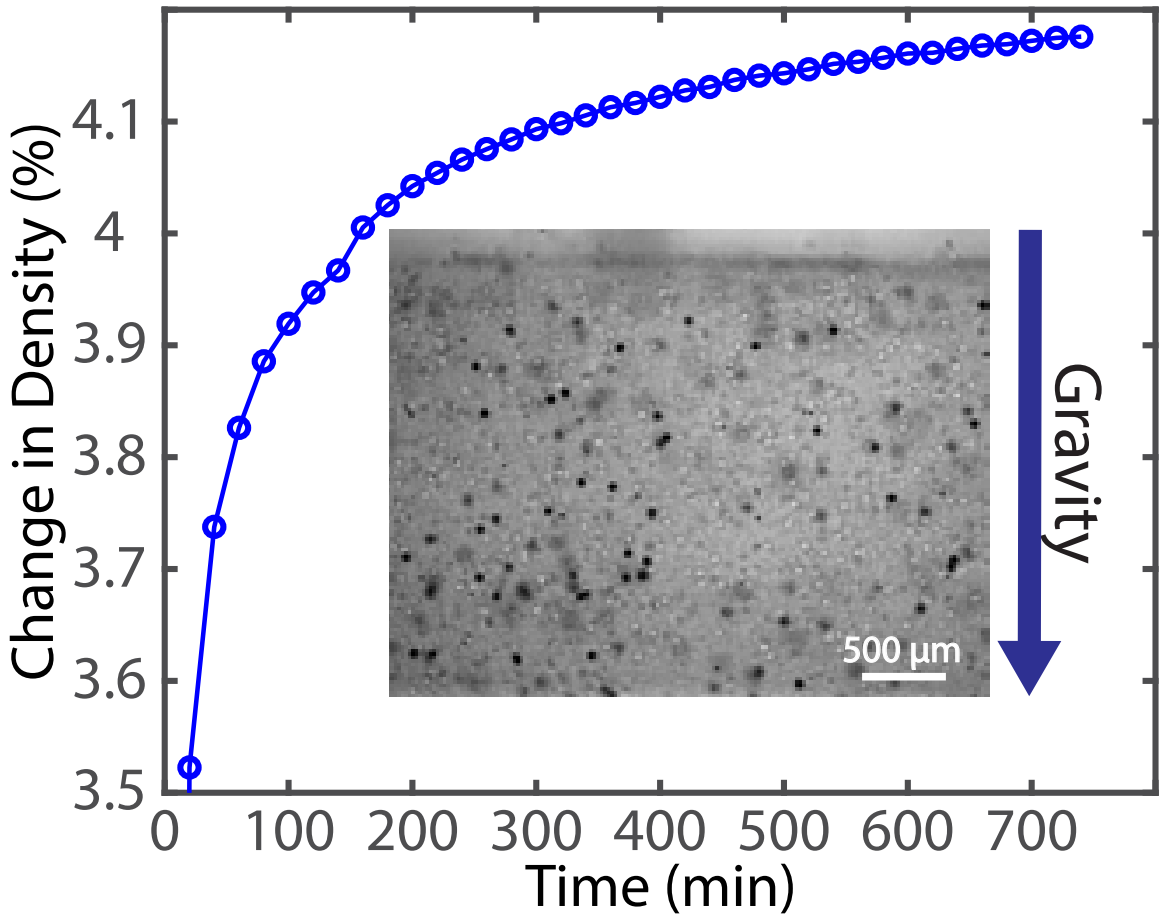

FIGURE 3.2. Sedimentation rates
Global change in density relative to the initially shaken sample versus time for a representative colloidal system. Even at the longest times studied the system is still slowly densifying. Inset: Image of the colloidal glass during sedimentation. The interstitial fluid has been index matched to the PMMA beads so they are nearly invisible. The black tracer particles are thus revealed.

polydispersity is chosen to frustrate crystallization. These colloids are suspended in a mixture of tetrahydronapthalene, decahydronapthalene, and cyclohexyl bromide. This three component liquid is chosen to allow for precise independent control of both the refractive index and density. To this are added a small number of dyed black polyethylene tracer colloids with the same density and diameter as the PMMA colloids (Cospheric BKPMS-1.2 45-53 um). This colloidal suspension is placed into a sealed cuvette sample chamber with an imaging width of 3 mm, large enough to allow for imaging far from any boundaries. The sealed cuvette allows us to reset the system to a new configuration by shaking it.

All imaging data was collected on a Nikon TE2000s microscope on a floating stage optical table in a climate controlled room. Illumination is provided by a high intensity red LED (Thorlabs M660D2) with output of 940 mW. High speed video was recorded on a Phantom Miro M310 high speed camera running at 64,000 fps using an image size of 192x192 pixels with a total collection of 110000 frames and a time of 1.72 s. We used a 50x lens (Nikon LU plan ELWD 50x/0.55 B ∞/0 WD 10.1) giving us an image resolution of 0.4μm per pixel. The cuvette being imaged is stabilized on the microscope using a custom sample holder that ensured a flat imaging plane and a minimum of vibration. The imaging stage is then encased in a small cardboard box for thermal and acoustic isolation.

We match the solutions' index to the PMMA, but introduce a slight density mismatch betweens the fluid and the colloids causing the colloids to slowly sediment, resulting in a colloidal glass whose packing fraction increases with increasing time. We measure the average sedimentation across many samples by imaging the whole cuvette as a function of time, as shown in figure 3.2 (Inset). We use particle image velocimetry to analyze the flow [59] to compute the change in

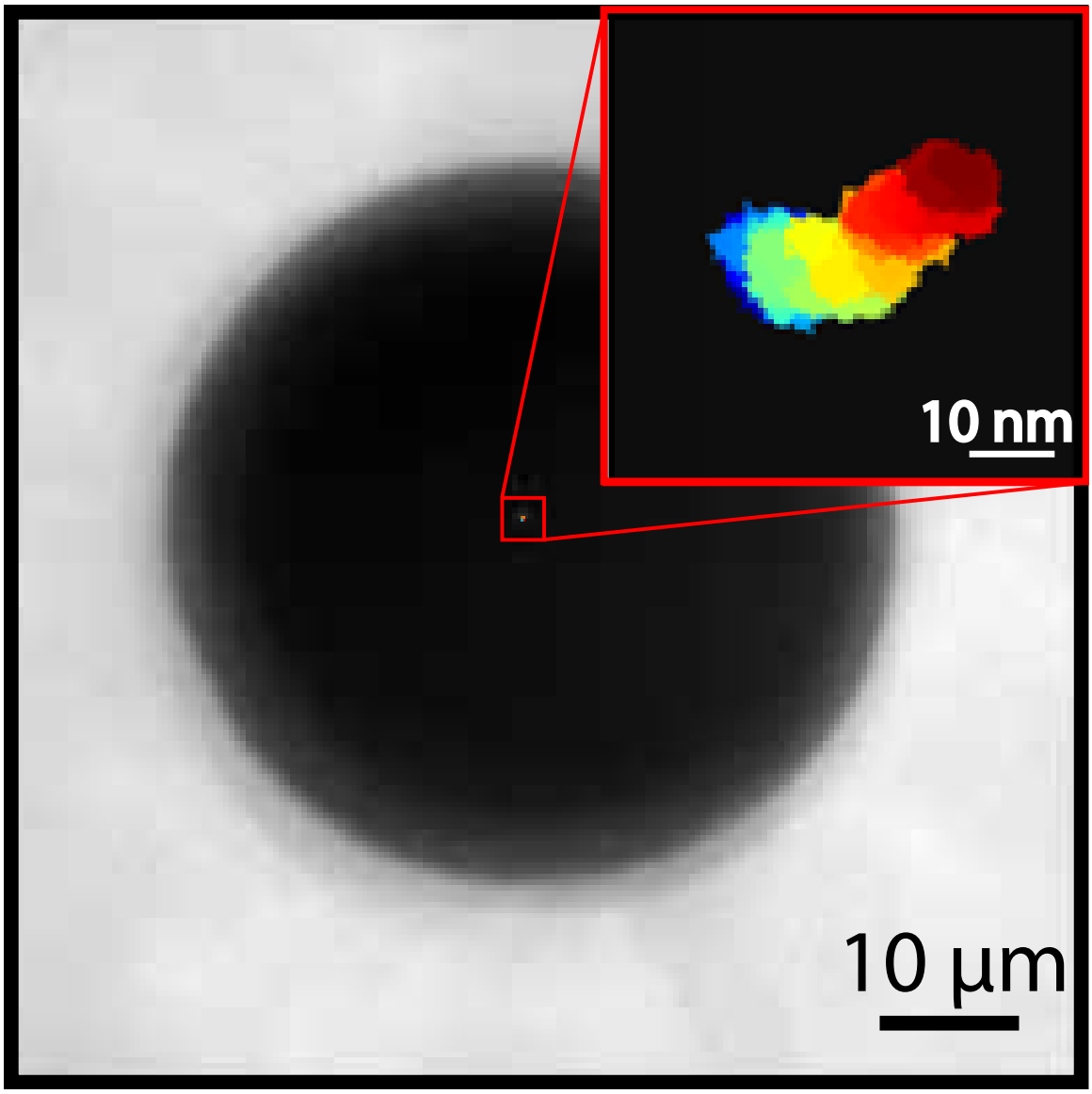

FIGURE 3.3. Tracer colloid in glass and path
Representative still image from the captured video showing the $\sim 50\mu$m diameter tracer-colloid inside the index matched colloidal glass. The tracked motion of the colloid for the entire 1.72 s video is overlayed on top of the colloid and blown up within the red box. The progression of time is represented by color running from start (blue) to end (dark red).

density versus time, a representative curve for which is shown in figure 3.2. The colloidal density always increases monotonically from the initial shaken state. The rate of densification slows over time but never stops. After the first hour the colloids have mainly fallen out of the solution and begin to compact more slowly. The total change in packing fraction over the course of 700 minutes of sedimentation is about 4%.

Due to the extreme vibration sensitivity of these measurements all data is collected late at night to ensure a minimum of human induced noise. Before imaging, the sample cuvette is vigorously shaken from multiple different directions in order to homogenize the colloidal suspension. Immediately afterwards it is placed in the cuvette holder on the microscope at which point a suitable tracer-colloid is selected and centered in the field of view of the camera. Tracer colloids are chosen no closer than 250 μm from the cuvette inner walls (approximately the diameter of 5 colloids away). Automated high speed video of the colloid is recorded every twenty minutes. Over the course of the first hour the tracer-colloid moves sufficiently that it is necessary to periodically move the stage to recenter the colloid. This motion is consistent with the large change seen in the sedimentation analysis. However, after reaching a sufficiently dense system, the tracer-colloid moves so little that the stage is locked down for all subsequent videos.

We use a radial center tracking algorithm [6] to find the center of the colloids motion in the plane perpendicular to gravity for every frame of the video. This tracking algorithm is unbiased and has a mean localization error of $\sim$ 1.5 nm for each frame. From this tracked data we compute the drift subtracted MSD for a

given video as:

$$\mathrm{MSD}(\tau) = \langle \|\vec{x}(t+\tau) - \vec{x}(t)\|^2 \rangle) - \|\langle \vec{x}(t+\tau) - \vec{x}(t) \rangle^2\| \tag{3.1}$$

where $\vec{x}(t)$ is the measured position of the particle at time t, τ is the lag-time between position measurements, and angle brackets denote a time average. Typically, the drift is an extremely small part of the MSD effecting only the long time (i.e. $\tau > 0.1$ s) motion. Because the localization error is independent and identically distributed we can subtract it from this MSD to achieve measurements below the nominal noise floor. This technique was employed and verified in previous work on the crossover from ballistic to diffusive motion in a freely floating colloid [13].

In order to distinguish between different forms of the MSD we begin by finding the lag time τ^* at which the presence of other particles begins to impinge upon the motion of the tracer. We characterize this as the time when each MSD deviates by more than 10% from the Clerx-Schram expression for free floating colloidal motion [12]. If the motion is logarithmic then beyond this lag time it should be well fit by

$$\mathrm{MSD}(\tau) = a \times \log\left(\frac{\tau}{\tau^*}\right) + x^* \tag{3.2}$$

where a characterizes the slope of the logarithm and x^* is the value of the MSD at τ^*.

3.3. Results and Discussion

As shown in figure 3.4, we find a substantial change of behavior with increasing time and thus increasing density. The MSD of the tracer-colloid just

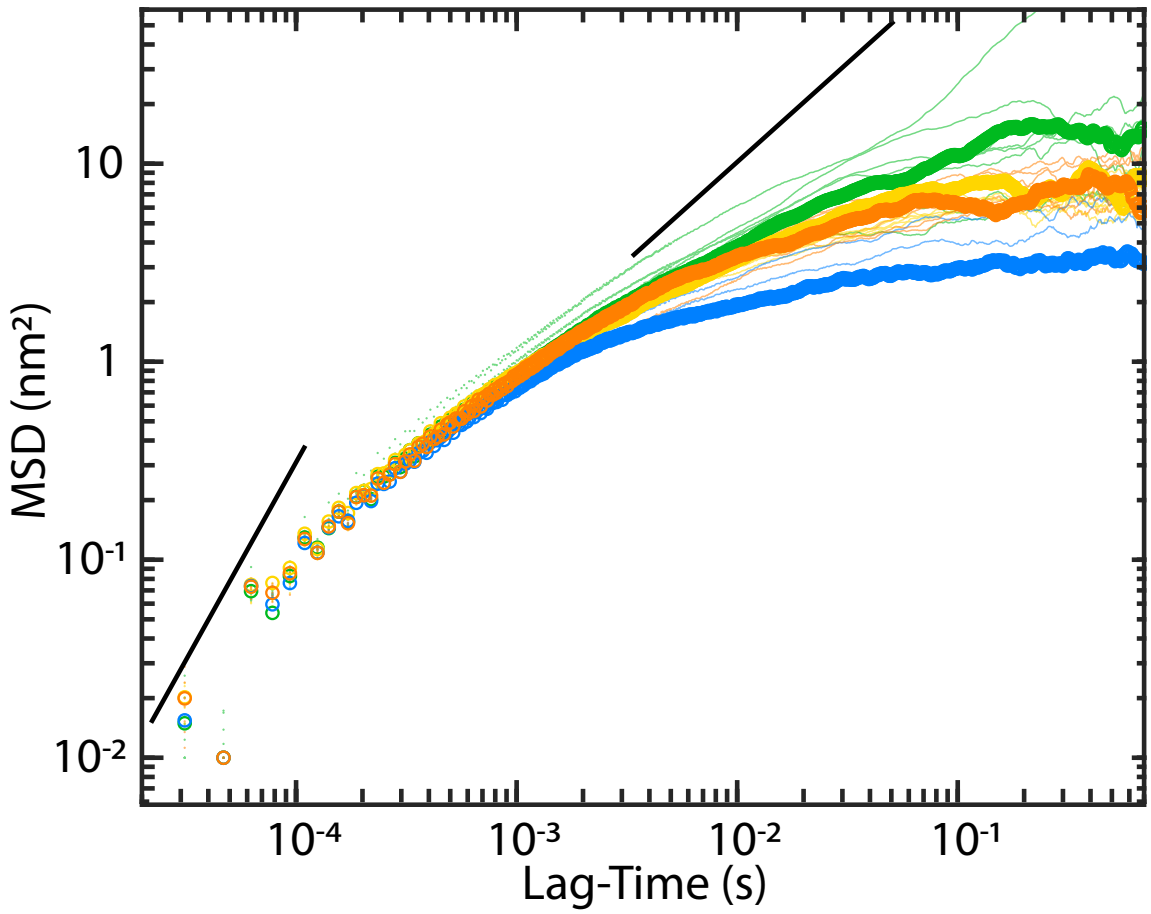

FIGURE 3.4. Mean squared displacement evolution in sedimenting glass MSDs from a sedimenting tracer-colloid plotted on a log-log scale. The MSDs were taken every 20 minutes. As a guide to the eye, we show ballistic and diffusive asymptotes demonstrating that at short times the motion is near ballistic and at long times the curves are all sub-diffusive. There are four important MSD regimes with a representative highlighted: from shaken to 160 minutes the MSD is sub-diffusive (green, 100 min), from 180 to 320 minutes the MSD is plateau (yellow, 200 min), between 320 and 400 minutes the MSD is logarithmic (lblue 400 min), from 420 to 520 minutes the MSD is plateau, which is nearly the same as the previous plateau (orange, 580 min).

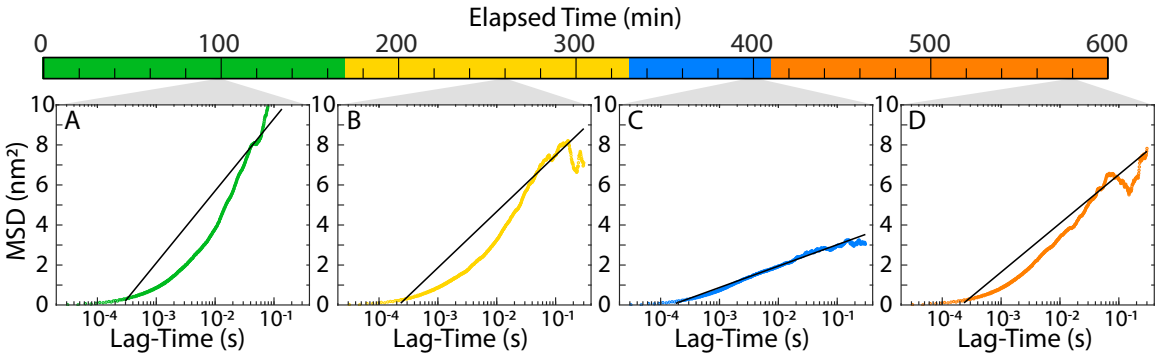

FIGURE 3.5. Logarithmic fit of mean squared displacement for different phases Representative MSD curves from the four time steps. Superimposed on each MSD is the best fit logarithm. A: MSD in the sub-diffusive regime, taken at 100 minutes with a logarithmic fit. B: MSD in plateau regime, 260 minutes. C: MSD in logarithmic regime, 400 minutes. D: MSD in reentrant plateau regime, 580 minutes.

after it has been shaken (green curves) shows ballistic motion at short times turning over to a subdiffusive motion at long times, consistent with that of a colloid in a dense liquid suspension. At lag times of around 2×10^{-4}s the MSD deviates from the expectation of a free floating thermal colloid [12] and instead shows sub-diffusive motion [50]. The absence of a diffusive regime results from the high initial colloidal density which leads to some caging even in a freshly shaken sample. As seen in figure 3.5A these MSDs are clearly not logarithmic.

As the colloidal density increases the power law of the sub-diffusive motion decreases towards zero. Starting at about 180 minutes the MSD flattens to a plateau, indicating that the tracer-colloid is trapped inside a cage of other colloids. This behavior is shown in yellow in figure 3.4 on a log-log scale and on a semi-log scale in figure 3.5B. This demonstrates that the system has entered into the stable glass phase. The height of the plateaus show a small but overall consistent trend towards smaller cages, driven by the slow overall densification of the system. The transition between ballistic motion and the plateau happens slowly, over nearly

three decades, only reaching the flat plateau at $\tau \sim 1 \times 10^{-1}$s. Across all samples measured, the transition from sub-diffusive to plateau happens after about 160 minutes.

After about 340 minute the constant plateau is replaced by an even lower MSD approaching that earlier plateau value, shown in blue in figure 3.4. As seen in figure 3.5C this motion is well fit by a logarithm. These are the only curves to demonstrate a good logarithmic fit. This behavior is indicative of the system entering the marginal glass phase. In some systems, the logarithmic MSD as a function of starting time exhibits a progression towards smaller values of the slope fitting parameter. This implies that small changes in packing fraction result in dramatic slowing down of dynamics. Across all samples measured, the transition from plateau to logarithmic happens after about 380 minutes.

The system remains in the marginal phase for about 80 minutes (across all samples, an average of 165 minutes). After which the MSDs consistently cease to be logarithmic and pop back up to a constant plateau, indicating a return to the stable glass regime, shown in orange curves in figures 3.4 and 3.5D. There is no further evolution of the MSD during the experimental observation.

Taken as a whole, the behavior of the densifying colloidal glass is consistent with the schematic phase diagram shown in Figure 3.1. The system begins in the liquid phase, at the point marked "X". The experiment proceeds at a constant temperature but increasing density along the red line, passing through the stable glass phase, the marginal phase, and ending once again in a high density stable glass as shown in figure 3.5. It is striking that not only do we see individual signatures of each phase but that they combine to begin to map out a phase diagram which agrees with the theoretical predictions.

3.4. Conclusions

We have created a colloidal glass at fixed temperature and tracked it through the liquid, stable glass, and marginal glass phases as a function of increasing density. We track an individual colloid deep within the glass at short times and find the associated MSD. This experiment lays the groundwork for a complete experimental determination of the glass phase diagram by repeating such measurements over as broad a range of temperatures as possible. Further, the techniques developed in this work explore a previously underlooked regime for glasses, that of the shortest time and length scales. Measuring behavior in this regime is a potent tool with which to explore previously inaccessible implications of the mean field theories of glasses and to probe new material properties. The experimental observation of these distinct phases provides strong evidence for the validity of the replica theory of glasses in physical systems.

CHAPTER IV

CONCLUSION

This work has focused on looking at the structures of materials that lurk along the border between solids and liquids. I have looked at both solid-like liquids and liquid-like solids by examining an embedded tracer's short time motion. I have designed and created an experimental apparatus that has the necessary precision, both temporal and positional, to detect the ballistic thermal motion of colloids. Using this apparatus I was then able to look at the transition out of ballistic motion of the mean squared displacement (MSD) to probe the structure of the material.

In chapter 2, I used colloidal test particles to examine the structure of two liquids: water and Cetyltrimethylammonium chloride (CTAC). Examining water first, I successfully found the short time ballistic asymptote, the first such measurement for a freely floating colloid. I then fit my experimentally measured MSD to the Clercx-Schram equation and confirmed that the temperature and radius were within the known ranges. This provides verification of my experimental technique proving its utility and correctness.

With the demonstrated results for water, a "simple" Newtonian liquid, I applied the same technique to looking at a Maxwell fluid, CTAC. I first verified that CTAC was a Maxwell fluid on the macro- scale using a rheometer. Then I examined the fluid on a micro-scale with a floating colloid as it moved from ballistic to diffusive motion. Qualitatively, my experimental MSD was similar to the predicted motion with a clear ballistic asymptote at short times, a plateau behavior at intermediate times, and diffusive motion at long times. However, when examined

quantitatively, it becomes clear that the MSD has been shifted significantly. The ballistic asymptote had been shifted likely due to a dramatic increase in the effective mass of the colloid. The plateau value was also lower indicating that the micro-scale interactions do not follow the macro-scale ones. This difference between the traditional macro scale experiments and my micro-scale experiment show that there is much left to be examined when examining liquids with solid like behaviors.

In the future, it may prove useful to expand on my work with liquids. One obvious expansion is to perform a more complete study of Maxwell liquids using not just different concentrations of CTAC, but also different Maxwell liquids. This would allow future researchers to make a detailed examination of the plateau values and track them to discover if the theory is incorrect or if only the CTAC mixture fails to follow the expected behavior. The other extension, and the one I pursued, was to examine the ballistic motion in a more densely packed system.

In chapter 3, I changed tack from looking at liquids to probing glasses. I created a colloidal glass with a refractive index matched, and slightly density mismatched interstitial liquid with embedded tracer colloids. Then, I tracked a tracer particle as the system sedimented, allowing me to probe the glass's structure at a fixed temperature and a range of packing densities. The resulting MSD moved through a series of different behaviors. The tracer colloid began with a ballistic to sub-diffusive transition indicating the glass was in the dense liquid phase. Next the colloid exhibited an MSD with a transition from ballistic to a flat plateau indicating it was trapped by it neighbors. This behavior is characteristic of a stable glass. After a further period of densification, the MSD moves to a long time logarithmically rising behavior meaning the system is in a marginal glass phase. This constitutes the first experimental realization of the marginal glass phase with

a thermal glass. Interestingly, if the system's packing density increases sufficiently, the MSD resumes the attributes of a stable glass. This last behavior shows the existence of a reentrant stable glass phase. This means the phase diagram for a colloidal glass has an unexpected level of complexity.

There are multiple ways in which the glass characterization experiment might be extended. Most obviously, the experiment might be used to make a fully fleshed out phase diagram for a colloidal glass. To perform this experiment it would be necessary to shift the effective temperature of the system perhaps, by changing the room temperature or changing the density mismatch. For such an experiment it would be useful to simultaneously track the sedimentation time with the tracer colloids motion. Second, this experiment could be expanded on by tracking multiple tracers. Doing so could be used as a probe of how homogeneous the system is, a question of some controversy [51]. Given the mixing that occurs for even small movements of the cuvette this expansion would probably be simplest with multiple camera systems, one for each particle. This might also be performed by putting the lenses and camera on a separate mechanically controlled stage. Finally, I would be curious to examine this system with colloids experiencing attractive or repulsive forces. This would add long range interactions into the system making them more relevant for molecular and metallic glasses. Interestingly, for strong long range interactions a marginal regime is not predicted and it would be interesting to try and verify these results [58]. Such an experiment would require some chemical synthesis of the colloidal system.

I began this work considering the chasm separating solid and liquids. I have worked to fill in the void between these two phases examining liquids that demonstrate solid components in chapter 2. Then I considered solids with liquid

like elements as discussed in chapter 3. In all of these materials I have shown that they are united at the short time limit by the thermal ballistic motion.

APPENDIX

EXPERIMENTAL APPARATUS

Here I have created a list of possible problems and where available my solutions. It also serves as a guide to the various software programs I have used, although most have an explanatory comment of their intended function. All of the software programs are in the Corwin lab Github repository. This is meant to act as an addendum to the various methods sections from the preceding chapters.

1. Cleaning the cuvette: When cleaning the cuvette, I generally start by flushing it with ethanol. For the corners where gunk collects, I use a syringe filled with ethanol to target a specific area. Often repetition is the only solution. Once the cuvette appears perfectly clean, but it often has small specks connected to the cuvette's inside, I dunk it inside a solution of piranha acid, an extremely dangerous mixture which should be used with care according to the methods given by the Parthasarathy Lab.

2. Colloidal glass: I mix the colloids with a mass of clear to black colloids at a ratio of 2,500.0/1.3 (mg). The interstitial liquid I use is made of Decalin (190.7μl), Tetralin (34.1μl) and Cyclohexyl Bromide (475.2μl). I use RefracIndexCalc.nb using Wiederseiner's review [60] to help determine the ration for index matching. All the solvents, but especially tetralin are dangerous and should be used exclusively in a fume hood and only removed in a sealed chamber. Once the liquid is mixed, I then mix the colloids and liquid at approximately an equal volume ratio. I shake the colloidal glass before adding it to the cuvette to increase the colloidal density. When adding the cuvette stopper it is important to wet it beforehand to eliminate/limit air pockets. With the stopper in place I seal

the cuvette with UV glue (Norland Optical Adhesive 61). If necessary the glue can be removed with Methylene Chloride bath. Once the cuvette has been sealed I use an optical wipe to clean the cuvette using ethanol (see method to clean optics).

3. Stability / Limiting Movement: One of the chief sources of error is the sample chamber vibrating. First I look at if the table the microscope is on is stabilized. If the table is floating, I'd like to check that the airflow is constant. You should also remove wires hanging off the table as much as possible. I have also found that if the stage is motorized a low level vibration is present if they're powered on. I have also found that air currents can cause the sample to vibrate. I generally fix this by encasing the sample in a box. If the cuvette or sample chamber glass is too thin the glass may vibrate. Another major source of vibrations are various fans, in particular the one on the camera although computer fans also contribute to noise. I typically run with the fan disconnected particularly if the movies are short. The camera will shut itself down if it gets too hot. A last point, is to move the automated switches away from the experiment lest they introduce a vibration.

4. Heating / Thermal Regulation: In order to minimize noise and make results more repeatable, keeping the system at a constant temperature is important. Nominally the experimental rooms are maintained at a constant temperature, although I'm skeptical of the precision. The major source of sample heating comes from the LED which should be off for as much time as possible. This also ensures that the LED doesn't overheat.

5. Experimental shifts to improve precision: The main experimental hit to precision is not having the tracer near the middle of the movie, or being out of focus. The light or the acquisition time should be adjusted to fill the camera's

signal range capacity. Precision is also improved by insuring that the illumination is as head-on as possible, basically check that the optics are properly aligned. The final piece is to keep all optical pieces as clean as possible.

6. Automated experimental image capture: The glass work has required automated image capture. To do this I use a NI digital IO USB controller to link two power switches (one for the LED and one for the camera) to the computer. The camera can be controlled through its Ethernet cable via Matlab (the camera companies software setup is included in the Github repository and is integrated into the automatic functions). The overarching Matlab control function is AutoExp.m, if using partitions AutoExpPart.m for sedimentation videos AutoWideView.m. These programs both automatically take experimental videos (cineAutoRun.m) and perform rough analysis of the videos (cineFunc.m). These programs are made up of other subsidiary function all of which have comments at the beginning explaining their use.

7. Post video capture analysis: The overall function for tracking and calculating the MSD is cinefunc.m. In addition I use fitting programs like goodLogFit.m, GlsLogFit.nb, or ClercxSchramFit.nb. All of these programs and the underlying functions are in the Corwin lab Github repository.

REFERENCES CITED

[1] Richard Johnston. World's slowest-moving drop caught on camera at last. *Nature News*. doi: 10.1038/nature.2013.13418.

[2] B. Luki, S. Jeney, C. Tischer, A. J. Kulik, L. Forr, and E.-L. Florin. Direct Observation of Nondiffusive Motion of a Brownian Particle. *Phys. Rev. Lett.*, 95(16):160601, October 2005. doi: 10.1103/PhysRevLett.95.160601.

[3] Tongcang Li, Simon Kheifets, David Medellin, and Mark G. Raizen. Measurement of the Instantaneous Velocity of a Brownian Particle. *Science*, 328(5986):1673–1675, June 2010. ISSN 0036-8075, 1095-9203. doi: 10.1126/science.1189403.

[4] Rongxin Huang, Isaac Chavez, Katja M. Taute, Branimir Luki, Sylvia Jeney, Mark G. Raizen, and Ernst-Ludwig Florin. Direct observation of the full transition from ballistic to diffusive Brownian motion in a liquid. *Nat Phys*, 7 (7):576–580, July 2011. ISSN 1745-2473. doi: 10.1038/nphys1953.

[5] Simon Kheifets, Akarsh Simha, Kevin Melin, Tongcang Li, and Mark G. Raizen. Observation of Brownian Motion in Liquids at Short Times: Instantaneous Velocity and Memory Loss. *Science*, 343(6178):1493–1496, March 2014. ISSN 0036-8075, 1095-9203. doi: 10.1126/science.1248091.

[6] Raghuveer Parthasarathy. Rapid, accurate particle tracking by calculation of radial symmetry centers. *Nat Meth*, 9(7):724–726, July 2012. ISSN 1548-7091. doi: 10.1038/nmeth.2071.

[7] Don S. Lemons and Anthony Gythiel. Paul Langevins 1908 paper On the Theory of Brownian Motion [Sur la thorie du mouvement brownien, C. R. Acad. Sci. (Paris) 146, 530533 (1908)]. *American Journal of Physics*, 65(11):1079–1081, November 1997. ISSN 0002-9505, 1943-2909. doi: 10.1119/1.18725.

[8] G. E. Uhlenbeck and L. S. Ornstein. On the Theory of the Brownian Motion. *Phys. Rev.*, 36(5):823–841, September 1930. doi: 10.1103/PhysRev.36.823.

[9] Robert Zwanzig and Mordechai Bixon. Hydrodynamic Theory of the Velocity Correlation Function. *Phys. Rev. A*, 2(5):2005–2012, November 1970. doi: 10.1103/PhysRevA.2.2005.

[10] Allan Widom. Velocity Fluctuations of a Hard-Core Brownian Particle. *Phys. Rev. A*, 3(4):1394–1396, April 1971. doi: 10.1103/PhysRevA.3.1394.

[11] E. J. Hinch. Application of the Langevin equation to fluid suspensions. *Journal of Fluid Mechanics*, 72(3):499–511, December 1975. ISSN 1469-7645, 0022-1120. doi: 10.1017/S0022112075003102.

[12] H. J. H. Clercx and P. P. J. M. Schram. Brownian particles in shear flow and harmonic potentials: A study of long-time tails. *Phys. Rev. A*, 46(4): 1942–1950, August 1992. doi: 10.1103/PhysRevA.46.1942.

[13] Andrew P. Hammond and Eric I. Corwin. Direct measurement of the ballistic motion of a freely floating colloid in Newtonian and viscoelastic fluids. *Phys. Rev. E*, 96(4):042606, October 2017. doi: 10.1103/PhysRevE.96.042606.

[14] Rachel E. Courtland and Eric R. Weeks. Direct visualization of ageing in colloidal glasses. *J. Phys.: Condens. Matter*, 15(1):S359–S365, December 2002. ISSN 0953-8984. doi: 10.1088/0953-8984/15/1/349.

[15] Laura J. Kaufman and David A. Weitz. Direct imaging of repulsive and attractive colloidal glasses. *The Journal of Chemical Physics*, 125(7):074716, August 2006. ISSN 0021-9606. doi: 10.1063/1.2227386.

[16] Gary L. Hunter and Eric R. Weeks. The physics of the colloidal glass transition. *Rep. Prog. Phys.*, 75(6):066501, 2012. ISSN 0034-4885. doi: 10.1088/0034-4885/75/6/066501.

[17] Eric R. Weeks. Introduction to the Colloidal Glass Transition. *ACS Macro Lett.*, 6(1):27–34, January 2017. doi: 10.1021/acsmacrolett.6b00826.

[18] E. Gardner. Spin glasses with p-spin interactions. *Nuclear Physics B*, 257: 747–765, January 1985. ISSN 0550-3213. doi: 10.1016/0550-3213(85)90374-8.

[19] Carolina Brito and Matthieu Wyart. Geometric interpretation of previtrification in hard sphere liquids. *The Journal of Chemical Physics*, 131(2):024504, July 2009. ISSN 0021-9606. doi: 10.1063/1.3157261.

[20] Giorgio Parisi and Francesco Zamponi. Mean-field theory of hard sphere glasses and jamming. *Rev. Mod. Phys.*, 82(1):789–845, March 2010. doi: 10.1103/RevModPhys.82.789.

[21] Patrick Charbonneau, Jorge Kurchan, Giorgio Parisi, Pierfrancesco Urbani, and Francesco Zamponi. Fractal free energy landscapes in structural glasses. *Nature Communications*, 5:3725, April 2014. ISSN 2041-1723. doi: 10.1038/ncomms4725.

[22] Silvio Franz, Giorgio Parisi, Pierfrancesco Urbani, and Francesco Zamponi. Universal spectrum of normal modes in low-temperature glasses. *PNAS*, 112 (47):14539–14544, November 2015. ISSN 0027-8424, 1091-6490. doi: 10.1073/pnas.1511134112.

[23] Giulio Biroli and Pierfrancesco Urbani. Breakdown of elasticity in amorphous solids. *Nature Physics*, 12(12):1130–1133, December 2016. ISSN 1745-2481. doi: 10.1038/nphys3845.

[24] Patrick Charbonneau, Jorge Kurchan, Giorgio Parisi, Pierfrancesco Urbani, and Francesco Zamponi. Glass and Jamming Transitions: From Exact Results to Finite-Dimensional Descriptions. *Annual Review of Condensed Matter Physics*, 8(1):265–288, 2017. doi: 10.1146/annurev-conmatphys-031016-025334.

[25] Ludovic Berthier, Giulio Biroli, Patrick Charbonneau, Eric I. Corwin, Silvio Franz, and Francesco Zamponi. Gardner physics in amorphous solids and beyond. *J. Chem. Phys.*, 151(1):010901, July 2019. ISSN 0021-9606. doi: 10.1063/1.5097175.

[26] Thomas Franosch, Matthias Grimm, Maxim Belushkin, Flavio M. Mor, Giuseppe Foffi, Lszl Forr, and Sylvia Jeney. Resonances arising from hydrodynamic memory in Brownian motion. *Nature*, 478(7367):85–88, October 2011. ISSN 0028-0836. doi: 10.1038/nature10498.

[27] John H. van Zanten and Karl P. Rufener. Brownian motion in a single relaxation time Maxwell fluid. *Phys. Rev. E*, 62(4):5389–5396, October 2000. doi: 10.1103/PhysRevE.62.5389.

[28] C. Wilhelm, J. Browaeys, A. Ponton, and J.-C. Bacri. Rotational magnetic particles microrheology: The Maxwellian case. *Phys. Rev. E*, 67(1):011504, January 2003. doi: 10.1103/PhysRevE.67.011504.

[29] M. Atakhorrami, D. Mizuno, G. H. Koenderink, T. B. Liverpool, F. C. MacKintosh, and C. F. Schmidt. Short-time inertial response of viscoelastic fluids measured with Brownian motion and with active probes. *Phys. Rev. E*, 77(6):061508, June 2008. doi: 10.1103/PhysRevE.77.061508.

[30] Yuriy L. Raikher, Victor V. Rusakov, and Rgine Perzynski. Brownian motion in a viscoelastic medium modelled by a Jeffreys fluid. *Soft Matter*, 9(45): 10857–10865, October 2013. ISSN 1744-6848. doi: 10.1039/C3SM51956B.

[31] T. G. Mason and D. A. Weitz. Optical Measurements of Frequency-Dependent Linear Viscoelastic Moduli of Complex Fluids. *Phys. Rev. Lett.*, 74(7): 1250–1253, February 1995. doi: 10.1103/PhysRevLett.74.1250.

[32] Matthias Grimm, Sylvia Jeney, and Thomas Franosch. Brownian motion in a Maxwell fluid. *Soft Matter*, 7(5):2076–2084, February 2011. ISSN 1744-6848. doi: 10.1039/C0SM00636J.

[33] Aneesur Rahman. Liquid Structure and SelfDiffusion. *The Journal of Chemical Physics*, 45(7):2585–2592, October 1966. ISSN 0021-9606, 1089-7690. doi: 10.1063/1.1727978.

[34] B. J. Alder and T. E. Wainwright. Decay of the Velocity Autocorrelation Function. *Phys. Rev. A*, 1(1):18–21, January 1970. doi: 10.1103/PhysRevA.1.18.

[35] Robert Zwanzig and Mordechai Bixon. Compressibility effects in the hydrodynamic theory of Brownian motion. *Journal of Fluid Mechanics*, 69(1): 21–25, May 1975. ISSN 1469-7645, 0022-1120. doi: 10.1017/S0022112075001280.

[36] L. D. Landau & E.M. Lifshitz. *Fluid Mechanics*, volume 6. Pergamon Press, 96-98, 1959. ISBN 0-08-029142-2.

[37] Kenji Aramaki, Suzuka Iemoto, Naoaki Ikeda, and Keitaro Saito. Composition-Insensitive Highly Viscous Wormlike Micellar Solutions Formed in Anionic and Cationic Surfactant Systems. *Journal of Oleo Science*, 59(4): 203–212, 2010. doi: 10.5650/jos.59.203.

[38] R. Oda, Janaky Narayanan, P. A. Hassan, C. Manohar, R. A. Salkar, F. Kern, and S. J. Candau. Effect of the Lipophilicity of the Counterion on the Viscoelasticity of Micellar Solutions of Cationic Surfactants. *Langmuir*, 14 (16):4364–4372, August 1998. ISSN 0743-7463. doi: 10.1021/la971369d.

[39] Mostafa H. Sharqawy, John H. Lienhard V, and Syed M. Zubair. Thermophysical properties of seawater: a review of existing correlations and data. *Desalination and Water Treatment*, 16(1-3):354–380, April 2010. ISSN 1944-3994. doi: 10.5004/dwt.2010.1079.

[40] B. U. Felderhof. Effect of the wall on the velocity autocorrelation function and long-time tail of Brownian motion in a viscous compressible fluid. *The Journal of Chemical Physics*, 123(18):184903, November 2005. ISSN 0021-9606, 1089-7690. doi: 10.1063/1.2084948.

[41] Patrick Charbonneau, Yuliang Jin, Giorgio Parisi, Corrado Rainone, Beatriz Seoane, and Francesco Zamponi. Numerical detection of the Gardner transition in a mean-field glass former. *Phys. Rev. E*, 92(1):012316, July 2015. doi: 10.1103/PhysRevE.92.012316.

[42] Ludovic Berthier, Patrick Charbonneau, Yuliang Jin, Giorgio Parisi, Beatriz Seoane, and Francesco Zamponi. Growing timescales and lengthscales characterizing vibrations of amorphous solids. *PNAS*, page 201607730, July 2016. ISSN 0027-8424, 1091-6490. doi: 10.1073/pnas.1607730113.

[43] Yuliang Jin and Hajime Yoshino. Exploring the complex free-energy landscape of the simplest glass by rheology. *Nature Communications*, 8:14935, April 2017. ISSN 2041-1723. doi: 10.1038/ncomms14935.

[44] C.L. Hicks, M.J. Wheatley, M.J. Godfrey, and M.A. Moore. Gardner Transition in Physical Dimensions. *Phys. Rev. Lett.*, 120(22):225501, May 2018. doi: 10.1103/PhysRevLett.120.225501.

[45] Beatriz Seoane and Francesco Zamponi. Spin-glass-like aging in colloidal and granular glasses. *Soft Matter*, 14(25):5222–5234, June 2018. ISSN 1744-6848. doi: 10.1039/C8SM00859K.

[46] Camille Scalliet, Ludovic Berthier, and Francesco Zamponi. Marginally stable phases in mean-field structural glasses. *Phys. Rev. E*, 99(1):012107, January 2019. doi: 10.1103/PhysRevE.99.012107.

[47] P. N. Pusey and W. van Megen. Observation of a glass transition in suspensions of spherical colloidal particles. *Phys. Rev. Lett.*, 59(18):2083–2086, November 1987. doi: 10.1103/PhysRevLett.59.2083.

[48] T. G. Mason and D. A. Weitz. Linear Viscoelasticity of Colloidal Hard Sphere Suspensions near the Glass Transition. *Phys. Rev. Lett.*, 75(14):2770–2773, October 1995. doi: 10.1103/PhysRevLett.75.2770.

[49] W. van Megen, T. C. Mortensen, S. R. Williams, and J. Mller. Measurement of the self-intermediate scattering function of suspensions of hard spherical particles near the glass transition. *Phys. Rev. E*, 58(5):6073–6085, November 1998. doi: 10.1103/PhysRevE.58.6073.

[50] Eric R. Weeks, J. C. Crocker, Andrew C. Levitt, Andrew Schofield, and D. A. Weitz. Three-Dimensional Direct Imaging of Structural Relaxation Near the Colloidal Glass Transition. *Science*, 287(5453):627–631, January 2000. ISSN 0036-8075, 1095-9203. doi: 10.1126/science.287.5453.627.

[51] Willem K. Kegel and and Alfons van Blaaderen. Direct Observation of Dynamical Heterogeneities in Colloidal Hard-Sphere Suspensions. *Science*, 287(5451):290–293, January 2000. ISSN 0036-8075, 1095-9203. doi: 10.1126/science.287.5451.290.

[52] Eric R Weeks and D. A Weitz. Subdiffusion and the cage effect studied near the colloidal glass transition. *Chemical Physics*, 284(1):361–367, November 2002. ISSN 0301-0104. doi: 10.1016/S0301-0104(02)00667-5.

[53] Ha Seong Kim, Nesrin enbil, Chi Zhang, Frank Scheffold, and Thomas G. Mason. Diffusing wave microrheology of highly scattering concentrated monodisperse emulsions. *PNAS*, 116(16):7766–7771, April 2019. ISSN 0027-8424, 1091-6490. doi: 10.1073/pnas.1817029116.

[54] H. G. E. Hentschel, Smarajit Karmakar, Edan Lerner, and Itamar Procaccia. Do athermal amorphous solids exist? *Phys. Rev. E*, 83(6):061101, June 2011. doi: 10.1103/PhysRevE.83.061101.

[55] Itamar Procaccia, Corrado Rainone, Carmel A. B. Z. Shor, and Murari Singh. Breakdown of nonlinear elasticity in amorphous solids at finite temperatures. *Phys. Rev. E*, 93(6):063003, June 2016. doi: 10.1103/PhysRevE.93.063003.

[56] A. Seguin and O. Dauchot. Experimental Evidence of the Gardner Phase in a Granular Glass. *Phys. Rev. Lett.*, 117(22):228001, November 2016. doi: 10.1103/PhysRevLett.117.228001.

[57] K. Geirhos, P. Lunkenheimer, and A. Loidl. Johari-Goldstein Relaxation Far Below ${T}_{g}$: Experimental Evidence for the Gardner Transition in Structural Glasses? *Phys. Rev. Lett.*, 120(8):085705, February 2018. doi: 10.1103/PhysRevLett.120.085705.

[58] Camille Scalliet, Ludovic Berthier, and Francesco Zamponi. Absence of Marginal Stability in a Structural Glass. *Phys. Rev. Lett.*, 119(20):205501, November 2017. doi: 10.1103/PhysRevLett.119.205501.

[59] William Thielicke and Eize Stamhuis. PIVlab Towards User-friendly, Affordable and Accurate Digital Particle Image Velocimetry in MATLAB. *Journal of Open Research Software*, 2(1):e30, October 2014. ISSN 2049-9647. doi: 10.5334/jors.bl.

[60] Sbastien Wiederseiner, Nicolas Andreini, Gal Epely-Chauvin, and Christophe Ancey. Refractive-index and density matching in concentrated particle suspensions: a review. *Exp Fluids*, 50(5):1183–1206, May 2011. ISSN 0723-4864, 1432-1114. doi: 10.1007/s00348-010-0996-8.